J. Am. Chem. Soc. **1986**, *108*, 1660–1671

Electron Nuclear Double Resonance (ENDOR) of Bis(imidazole)-Ligated Low-Spin Ferric Heme Systems

Charles P. Scholes,* Krzysztof M. Falkowski, Shirley Chen, and Janet Bank

Contribution from the Department of Physics and Center for Biological Macromolecules, State University of New York at Albany, Albany, New York 12222. *Received June 10, 1985*

Abstract: The ENDOR (electron nuclear double resonance) technique was used to obtain intimate electronic information on nitrogens and protons in bis(imidazole)ferric porphyrin systems, both model and protein. The purposes of this work were to assign characteristic ENDOR from particular nuclei, to probe electron density at these nuclei, to gain insight into the geometry of the bis(imidazole) heme system, and to probe for protein-induced perturbation to the basic bis(imidazole) ferric heme structure. Hyperfine coupling to the Fe-liganding imidazole nitrogen was seen and assigned for the first time in any low-spin ferric heme system, and its best resolution was with ^{15}N-enriched imidazole. Combinations of porphyrin and imidazole containing either naturally occurring ^{14}N or isotopically enriched ^{15}N were used to measure the overall heme and imidazole nitrogen hyperfine coupling. This coupling was found to be highly isotropic when measured as a function of the electronic g value. The isotropic couplings for ^{15}N heme and imidazole were, respectively, 7.4 and 7.8 MHz in magnitude. Anisotropy, about equal to 10% of the isotropic coupling, was noted as a function of electronic g value. ^{14}N quadrupole couplings along the g_z direction normal to the heme were noted for both heme and imidazole nitrogen and compared to the corresponding values found from other heme systems. Electronic inequivalence of heme nitrogens was seen in myoglobin imidazole. Meso proton ENDOR was observed from a number of heme systems. Proton ENDOR from pyrrole and phenyl protons was assigned in bis(imidazole)ferric tetraphenylporphine [(TPP)Fe(Im)$_2^+$] through the use of selectively deuterated TPP's. A surprising electronic inequivalence of pyrrole protons was noted by ENDOR and was due to differing contact interactions from unequal amounts of unpaired electron spin reaching various pyrrole proton positions. TPP formally has 4-fold molecular symmetry and physical equivalence of its eight pyrrole protons; so the electronic inequivalence noted by ENDOR appears to propagate out from the ferric iron, whose symmetry as shown by its rhombic g values of g_z, g_y, and g_x = 2.92, 2.30, and 1.56 is lower than 4-fold. Proton ENDOR from the two imidazole protons adjacent to the Fe-liganding nitrogen was assigned through selectively deuterated imidazoles and extensively followed as a function of electronic g value. The best resolution of ENDOR from these protons occurred at a nonprincipal g value (2.4–2.5), and the observed ENDOR frequencies were well correlated with dipolar coupling to the electron spin on the iron and contact coupling from the spin on the adjacent imidazole carbons. The ENDOR from these protons, when observed at the minimal electronic g value of g_x, indicated an imidazole plane at approximate right angles to the g_x direction. Similar, but definitely not identical, spectra to those seen from these two protons in (TPP)Fe(Im)$_2^+$ were observed in the bis(imidazole) heme proteins myoglobin imidazole, cytochrome b_5, and cytochrome a; the implication is that there are protein-induced differences in imidazole ligation. ENDOR evidence for the exchangeable proton on the nonligated nitrogen of imidazole was seen in myoglobin imidazole from the exogenously added imidazole.

Histidine with its imidazole side chain is a ubiquitous heme protein ligand. An important pathway for modulation of the heme's electronic properties is via the imidazole ligand(s). Such modulation may affect important functions such as the strength of O_2 binding[1] or the redox behavior of the metal center.[2] Tension at the Fe–imidazole bond[3a–c] and/or change in the orientation of the imidazole plane with respect to the heme[4a,b] are plausible mechanisms by which the imidazole can affect the heme electronic structure.

Electronic properties of low-spin ferric heme systems are intimately shown by hyperfine couplings between unpaired electron spins centered at the heme iron and nearby nuclear spins. Very near nuclei like the liganding nitrogens can experience large hyperfine couplings because of the spin that arrives directly on them in a covalent fashion.[5] More distant nuclei such as protons of heme and of axial imidazole can additionally interact with the electron spin via electron nuclear dipolar coupling from which the iron–proton distance and orientation of the proton may become known.[6]

The technique which we use to resolve hyperfine couplings is electron nuclear double resonance (ENDOR). When nuclear spins are hyperfine coupled to electron spins, the ENDOR technique monitors the change in the EPR signal that results when these nuclei are flipped by a radio frequency (rf) field. The information so obtained is similar to what one might obtain by solid-state NMR applied to the same nuclei but with the much greater sensitivity of EPR. Because it measures contact interactions and some aspects of dipolar couplings (pseudocontact interactions), high-resolution NMR of protons is a useful complementary technique to ENDOR. However, under liquid conditions, rapid fluctuations of the g-tensor direction and chemical exchange may cause difficulty in interpreting NMR data;[4b] on the other hand, high-resolution proton NMR can directly measure the sign of the contact interactions. We have found that ENDOR has a particular advantage for studying the environs of metal centers in high molecular weight proteins where there are nuclei that experience large hyperfine couplings and thus would have short relaxation times and broad NMR lines even in liquid.

Our ENDOR experiments were intended to probe the structure of the bis(imidazole) heme center for several mutually complementary reasons. These reasons are as follows: 1. to discover and assign ENDOR transitions, e.g., of ^{15}N on imidazole and of specific protons on heme and imidazole; 2. to use ENDOR as an analytical tool to probe for the existence of the imidazole ligand; 3. to use ENDOR to probe the electronic distribution about the heme through detailed resolution of the hyperfine and quadrupole tensors of particular nuclei; 4. to obtain evidence for nearby exchangeable protons; 5. to obtain evidence for the angular orientation of the electronic g tensor with respect to the imidazole planes; and 6. to discover evidence for biologically relevant, protein-induced

* To whom correspondence should be addressed.

(1) (a) Perutz, M. F.; Ladner, J. E.; Simon, S. R.; Ho, C. *Biochemistry* **1974**, *13*, 2163–2173. (b) Perutz, M. F.; Heidner, E. J.; Ladner, J. E.; Beetlestone, J. G.; Ho, C.; Slade, E. F. *Ibid.* **1974**, *13*, 2187–2200.

(2) Walker, F. A.; Balke, V. L.; McDermott, G. A. *J. Am. Chem. Soc.* **1982**, *104*, 1569–1574.

(3) (a) Goff, H. *J. Am. Chem. Soc.* **1980**, *102*, 3252–3254. (b) Geibel, J.; Cannon, J.; Campbell, D.; Traylor, T. G. *Ibid.* **1978**, *100*, 3575–3585. (c) Walker, F. A. *J. Am. Chem. Soc.* **1980**, *102*, 3254–3256.

(4) (a) Traylor, T.; Berzinis, A. P. *J. Am. Chem. Soc.* **1980**, *102*, 2844–2846. (b) Shulman, R. G.; Glarum, S. H.; Karplus, M. *J. Mol. Biol.* **1971**, *57*, 93–115.

(5) Mulks, C. F.; Scholes, C. P.; Dickinson, L. C.; Lapidot, A. *J. Am. Chem. Soc.* **1979**, *101*, 1645–1654.

(6) Scholes, C. P. In "Multiple Electron Resonance Spectroscopy"; Dorio, M. M., Freed, J. H., Eds.; Plenum Press: New York, 1979; Chapter 8.

0002-7863/86/1508-1660$01.50/0

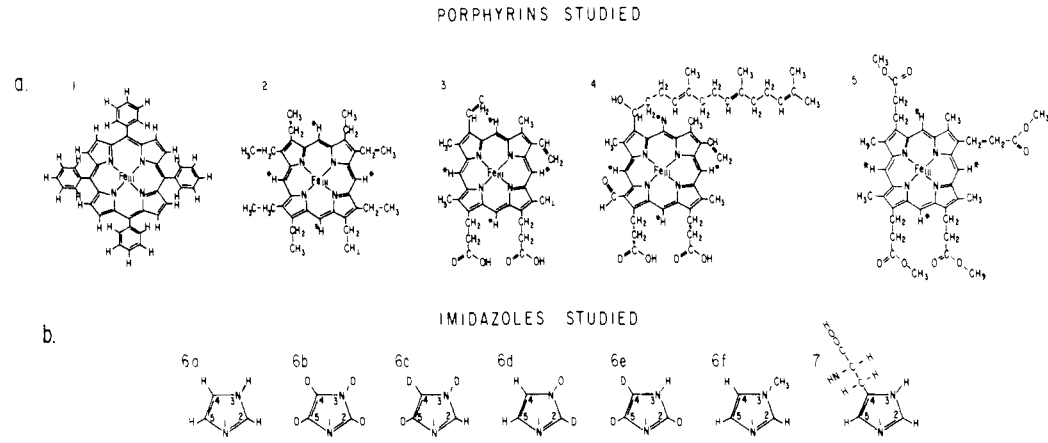

Figure 1. Structures of the porphyrin systems studied: **1**, ferric tetraphenylporphine; **2**, ferric octaethylporphine; **3**, ferric protoporphyrin; **4**, ferric heme A; **5**, ferric coproporphyrin tetramethyl ester. **1**, **2**, and **5** were studied as bis(imidazole) models; **3** was studied in cytochrome b_5 and MbIm and **4** in cytochrome *a*. Structures of imidazoles used in this study: **6a**, fully protonated imidazole; **6b**, fully deuterated imidazole; **6c**, 3,4,5-trideuterioimidazole; **6d**, 2,3-dideuterioimidazole; **6e**, 2,4,5-trideuterioimidazole; **6f**, 3-methylimidazole; **7**, histidine.

perturbations to the basic bis(imidazole) heme structure.

This initial work has partly focused on porphyrin model systems. In particular bis(imidazole)tetraphenylporphine was studied because its X-ray structure is known,[8] because there was previous high-resolution proton NMR work on it,[7,9] and because there is relative ease of selective deuteration of the porphyrin and imidazole moieties. Ferric coproporphyrin tetramethyl ester, isotopically enriched with ^{15}N on the pyrroles, was valuable in distinguishing the ENDOR of the heme nitrogen from imidazole nitrogen. Studies were also done on myoglobin imidazole as a "model" protein where the water sixth ligand of aquometmyoglobin has been replaced by an exogenous imidazole. The structure of myoglobin imidazole[10] and the orientation of its *g* tensor with respect to the heme are known.[11] Calf liver cytochrome b_5 whose X-ray structure is known[12] was studied, and finally cytochrome *a* of cytochrome *c* oxidase, whose heme ligation is thought to be bis(imidazole),[13a-d] was studied. A reason for these protein studies was to compare ENDOR results from the bis(imidazole)-ligated heme in three different proteins.

All these systems, model and protein, have fairly similar *g* factors, implying a relatively unstrained bis(imidazole) coordination.[14a,b] These are not systems with the "highly anisotropic low-spin" (HALS) configuration which a number of heme proteins and complexes have;[15a,b] such HALS proteins are clearly appropriate subjects for future ENDOR study as are systems with deprotonated imidazolate ligation.[16] In this present work, we have attempted to lay the foundation for understanding the ENDOR of hyperfine couplings to protons and nitrogens in bis(imidazole) heme systems and have pointed in directions where ENDOR can be used to probe biological perturbations and differences between heme proteins.

Experimental Section

Chemicals. The structures of the porphyrins and imidazoles used are shown in Figure 1. Ferric tetraphenylporphine (TPP)Fe^{III} (Figure 1, **1**) and ferric octaethylporphine (OEP)Fe^{III} (Figure 1, **2**) were purchased as the chloride derivatives from Strem Chemical Co. and used without further purification. Selectively deuterated ferric TPP's were a kind gift of Prof. H. M. Goff, Department of Chemistry, University of Iowa. These were either D-20 (99%) which is deuterated on the phenyl groups but not on the pyrroles, or D-8 (85%), which is deuterated on the pyrroles but not the phenyls. Ferric coproporphyrin tetramethyl ester [(COP)Fe^{III}] (Figure 1, **5**) with ^{15}N incorporated biosynthetically at a 75–85% enrichment was a kind gift of Prof. J. Peisach, Albert Einstein Medical College. This synthesis was originally performed by Porphyrin Products, Logan, UT. Standard ^{14}N ferric coproporphyrin tetramethyl ester was also purchased from Porphyrin Products. Standard imidazole (Figure 1, **6a**) with ^{14}N and ^{1}H in ~100% abundance was purchased from Sigma and recrystallized from benzene. [^{15}N]Imidazole (99% ^{15}N) was purchased from Stohler Chemical and was recrystallized from benzene. 1-Methylimidazole (Figure 1, **6f**) was purchased from Sigma. Fully deuterated (D-4, 98%) imidazole (Figure 1, **6b**) was purchased from Stohler. Selectively deuterated imidazoles (Figure 1, **6c–e**) were prepared by the method of ref 17. These were checked for deuteration by NMR, and the deuteration was found to be 99.8% complete. Deuterated buffer was prepared with 99.9% D_2O, but overall deuteration of this buffer would be slightly less because nondeuterated phosphate salts were used in preparing the buffer. Deuterated CD_2Cl_2 and $CDCl_3$ (99.8% deuterated) were purchased from Merck.

Sperm whale metmyoglobin, (Mb) Sigma Type II, was further purified by chromatography on Whatman DE-52.[18] Exchangeable protons on myoglobin were deuterated by soaking with a 5-fold volume excess of deuterated buffer followed by reconcentration with an Amicon filtration device; exchange and reconcentration were done twice over the period of a day to achieve an expected deuteration of about 95%. Calf liver cytochrome b_5, prepared by the method of ref 19, was a kind gift of Prof. Grant Mauk, Department of Biochemistry, University of British Columbia. Bovine cytochrome *c* oxidase was prepared by the method of ref 20a with modification as described in ref 20b. Oxidase typically contained 100 mg of protein/mL with a copper-heme *a* ratio in the 1.0–1.1 range, with 11 nmol of heme *a*/mg of protein and with about 20% by weight phospholipid. The oxidase sample was dissolved in 1% sodium cholate, 50 mM phosphate buffer, pH 7.4.

Imidazole derivatives of the porphine models were prepared by addition of a 10:1 mole ratio of imidazole to a 3 mM porphine solution. The solvent was a 1:1 mixture of chloroform/methylene chloride, which formed a glass on freezing. A 10-fold molar excess of imidazole was added to metmyoglobin to give the imidazole myoglobin. Samples of the myoglobin and cytochrome b_5 were prepared in 50:50 mixtures of buffer

(7) La Mar, G. N.; Walker, F. A. *J. Am. Chem. Soc.* **1973**, *95*, 1782–1790.
(8) Collins, D. M.; Countryman, R.; Hoard, J. L. *J. Am. Chem. Soc.* **1972**, *94*, 2066–2078.
(9) Satterlee, J. D.; La Mar, G. N. *J. Am. Chem. Soc.* **1976**, *98*, 2804–2808.
(10) Bolognesi, M.; Cannillo, E.; Ascenzi, P.; Giacometti, G. M.; Merli, A.; Brunori, M. *J. Mol. Biol.* **1982**, *158*, 305–315.
(11) Hori, H. *Biochim. Biophys. Acta* **1971**, *251*, 227–235.
(12) Mathews, F. S.; Czerwinski, E. W.; Argos, P. In "The Porphyrins:, Vol. VII", Dolphin, D., Ed.; Academic Press: New York, 1979; Part B, Chapter 3.
(13) (a) Blumberg, W. E.; Peisach, J. In "Probes of Structure and Function of Macromolecules and Membranes"; Chance, B., Yonetani, T., Mildvan, A. S., Eds.; Academic Press: New York, 1971; Vol. 2, pp 215–239. (b) Babcock, G. T.; Callahan, P. M.; Ondrias, M. R.; Salmeen, I. *Biochemistry* **1981**, *20*, 959–966. (c) Babcock, G. T.; Vickery, L. E.; Palmer, G. *J. Biol. Chem.* **1976**, *251*, 7907–7919. (d) Eglinton, D. G.; Hill, B. C.; Greenwood, C.; Thomson, A. J. *J. Inorg. Biochem.* **1984**, *21*, 1–8.
(14) (a) Walker, F. A.; Reis, D.; Balke, V. L. *J. Am. Chem. Soc.* **1984**, *106*, 6888–6898. (b) Peisach, J.; Blumberg, W. E.; Adler, A. D. *Ann. N. Y. Acad. Sci.* **1973**, *206*, 310–327.
(15) (a) Salerno, J. C.; Leigh, J. S. *J. Am. Chem. Soc.* **1984**, *106*, 2156–2159. (b) Migita, C.; Iwaizumi, M. *Ibid.* **1981**, *103*, 4378–4381.
(16) Quinn, R.; Nappa, M.; Valentine, J. S. *J. Am. Chem. Soc.* **1982**, *104*, 2588–2595.
(17) (a) Vaughan, J. D.; Mughrabi, Z.; Wu, E. C. *J. Org. Chem.* **1970**, *35*, 1141–1145. (b) Van Camp, H. L.; Sands, R. H.; Fee, J. A. *J. Chem. Phys.* **1981**, *75*, 2098–2107.
(18) Scholes, C. P.; Isaacson, R. A.; Feher, G. *Biochim. Biophys. Acta* **1972**, *263*, 448–452.

(pH or pD 6.8, 0.05 M phosphate) to glycerol since the presence of glycerol helps to form a glassy matrix which prevents the aggregation of paramagnetic centers that interferes with the ENDOR process. Both the myoglobin and cytochrome b_5 were about 3 mM in heme, while the cytochrome *c* oxidase was about 0.6 mM in cytochrome *a*.

Instrumentation. EPR spectra were obtained with a Bruker ER 420 spectrometer equipped for low power dispersion operation and equipped with a home-built low-temperature microwave head and liquid helium double-Dewar. Details of the ENDOR apparatus are given in ref 6 and 21. *g*-value measurements were obtained under nonsaturating absorption (χ'') conditions at 77 K using 100-kHz field modulation of about 4 G p.t.p. (peak to peak). ENDOR was done exclusively in the dispersion (χ') mode under rapid passage conditions at liquid helium temperatures. In our method of doing ENDOR, we monitor the ENDOR-induced change in the rapid-passage 100-kHz field-modulated EPR signal as we sweep the frequency of the rf field. The results of repetitive rf sweeps are stored in the memory of a Tracor 570 Signal Averager and then either printed out on an *X*–*Y* recorder or transferred for storage on magnetic disk to a Z-80-based microcomputer. The ENDOR signals which we generally show are simply the rf-induced ENDOR changes in the 100-kHz rapid-passage signal. However, we occasionally have wanted to enhance certain spectral features, e.g., shoulders, and have done so by taking a derivative with respect to the radio frequency of our preexisting ENDOR signal in the microcomputer.

For the myoglobin imidazole and cytochrome b_5, the best temperature for good proton ENDOR signal-to-noise and spectral resolution was 4.2 K, while for the porphine models and cytochrome *a* the best temperature was found to be 2.1 K. Optimum ^{14}N and ^{15}N ENDOR was obtained with a 100-kHz field modulation amplitude of 2 G p.t.p. The strongly coupled imidazole protons with couplings of the order 2–5 MHz were best obtained with 100-kHz field modulation of about 0.8 G p.t.p., while more weakly coupled protons were obtained with field modulation in the 0.2–0.4-G p.t.p. range. ENDOR rf fields of about 0.5 G p.t.p. were used. Microwave powers of 1–10 μW were employed.

The ENDOR signal arises from rf-induced perturbation to the electron nuclear spin population when it is subject to saturating microwave power. Detailed mechanisms for the ENDOR process in solids depend on several different spin relaxation processes, and many of these are temperature-dependent, e.g., spin–lattice relaxation.[6] For the samples studied at the temperatures used, we have found by pulsed saturation recovery EPR the electron T_1's to be in the 10-ms regime.[22] Factors which we vary to optimize the ENDOR signal are discussed in ref 6, pp 306–307. Because we are not intimately familiar with all the coupled processes that affect the ENDOR signal, we proceed on the basis of experience. Thus, it is not always possible to give a complete explanation of why a particular ENDOR transition has low intensity, e.g., the lower member of a ^{14}N or ^{15}N Zeeman pair in low-spin ferric heme.[5] In interpreting our data, we must rely on the ENDOR signals that we do see, on experience, on isotopic substitution, and sometimes on correlations with other techniques such as electron spin echo spectroscopy or high-resolution NMR.

Theoretical Background

Low-spin ferric heme systems have a rhombic *g* tensor whose g_z direction has been found near the heme normal, while the g_x and g_y directions lie near the heme plane.[11] The *g* tensor of this five-electron system is quantitatively related to the respective orbital coefficients (*a*, *b*, and *c*) of those metal d_{yz}, d_{xz}, and d_{xy} orbitals which participate in the effective ground spin doublet.[23,24] In the d_{yz}, d_{xz}, and d_{xy} manifold, the majority of unpaired electron spin (≈90% for the case of bis(imidazole) ferric heme) lies in the highest d_{yz} orbital with progressively lesser amounts in the d_{xz} and d_{xy} orbitals. The difference in ligand field strength between the in-plane (heme) and out-of-plane (axial) ligands causes the d_{xy} orbital to be separated from the d_{xz} and d_{yz} orbitals by a "tetragonal splitting". The d_{xz} and d_{yz} orbitals are separated from each other by a "rhombic splitting". The review of ref 23 and discussion in ref 14a and 24 give quantitative discussion of the relation between the *g* tensor, orbital coefficients (*a*, *b*, and *c*), and the tetragonal and rhombic splittings.

The reason for the splitting of the d_{xz} and d_{yz} orbitals is not clear; the present work may shed light on this problem. It has been suggested that preferential π bonding of an axial ligand orbital to the d_{yz} orbital would raise the energy of the d_{yz} orbital.[23] The preferential direction for imidazole π ligand-to-metal bonding would be perpendicular to the imidazole plane, and this perpendicular direction would establish the *y* direction. Conceivably π metal-to-ligand back-bonding could act instead to preferentially lower the energy of the d_{xz} orbital, in which case the *x* direction would be the direction perpendicular to the plane of the imidazole that most strongly π back-bonds. The π-bonding or -back-bonding direction would be unambiguously determined in the case of bis(imidazole) heme systems if the planes of the two imidazoles were parallel to each other or if one of the imidazoles were more tightly bound to the heme iron with a shorter Fe–N bond.

With the ENDOR technique, we measure transitions between nuclear spin levels which have been split by electron nuclear hyperfine interactions, nuclear quadrupole interactions, and the nuclear Zeeman interaction. The overall nuclear spin Hamiltonian is thus

$$\mathcal{H}_{\text{nuclear}} = A_{xx}I'_xS'_x + A_{yy}I'_yS'_y + A_{zz}I'_zS'_z - g_n\beta_n\vec{H}\cdot\vec{I} + Q_{xx}I'^2_x + Q_{yy}I'^2_y + Q_{zz}I'^2_z \quad (1)$$

The terms in A_{zz}, A_{xx}, and A_{yy} are the hyperfine terms where the components of each term may contain both anisotropic (dipolar) and contact interactions. The primes indicate that hyperfine axes need not coincide with *g*-tensor axes. The next term in $g_n\beta_n\vec{H}$ is the direct Zeeman interaction with the applied magnetic field and the final term in Q_{zz}, Q_{xx}, and Q_{yy} shows the nuclear quadrupole interaction. First-order expressions for ENDOR frequencies will approximately hold along *g*-tensor directions if hyperfine and quadrupole axes are colinear and at other orientations if the hyperfine or direct Zeeman interaction should dominate the nuclear Hamiltonian. If one takes the magnetic field along a *z* direction which coincides with quadrupole and hyperfine axes, then to first order

$$(I = \tfrac{1}{2}) \quad \nu_{\text{ENDOR}} = |\tfrac{1}{2}A_{zz} \pm \nu_0| \quad (2a)$$

$$(I = 1) \quad \nu_{\text{ENDOR}} = \tfrac{1}{2}|A_{zz}| \pm \tfrac{3}{2}|Q_{zz}| \pm \nu_0 \quad (2b)$$

where ν_0 is the appropriate free nuclear NMR frequency. In cases where the hyperfine term dominates (e.g., ^{14}N and ^{15}N), one often finds pairs of ENDOR lines split by $2\nu_0 = 2g_n\beta_nH$, where g_n is the appropriate nuclear *g* value and β_n is the nuclear Bohr magneton. In cases where the nuclear Zeeman interaction dominates (e.g., protons), one finds pairs of ENDOR lines separated by $|A_{zz}|$ and centered at the free nuclear NMR frequency. Details of more general higher order expressions for the ^{15}N and ^{14}N ENDOR frequencies in single crystals of high-spin ferric heme systems and the relation of the derived hyperfine and quadrupole couplings to electron density are given in ref 25.

A hyperfine coupling of considerable importance is the through-space dipolar coupling between electron spin, assumed concentrated at the iron where the majority (but not necessarily 100%) of the electron spin resides, and a proton nucleus. Such coupling depends on angles between the magnetic field and the vector from the iron to the proton. The general form for such a dipolar interaction between electron and proton magnetic moments is[26]

$$\mathcal{H}_{\text{dipolar}} = \vec{\mu}_e\cdot\vec{\mu}_n/r^3 - 3(\vec{\mu}_e\cdot\vec{r})(\vec{\mu}_n\cdot\vec{r})/r^5 \quad (3)$$

where $\vec{r}$ is the electron to proton vector, $\vec{\mu}_e$ is the electron magnetic moment, and $\vec{\mu}_n$ is the nuclear magnetic moment. For the case at hand, which includes *g* anisotropy,

(19) Reid, L. S.; Mauk, A. G. *J. Am. Chem. Soc.* **1982**, *104*, 841–845.
(20) (a) Kuboyama, M.; Yong, F. C.; King, T. E. *J. Biol. Chem.* **1972**, *247*, 6375–6383. (b) Yu, C.; Yu, L.; King, T. E. *Ibid.* **1975**, *250*, 1383–1392.
(21) LoBrutto, R.; Wei, Y-H.; Mascarenhas, R.; Scholes, C. P.; King, T. E. *J. Biol. Chem.* **1983**, *258*, 7437–7448.
(22) Scholes, C. P.; Janakiraman, R.; Taylor, H.; King, T. E. *Biophys. J.* **1984**, *45*, 1027–1030.
(23) Palmer, G. In "Iron Porphyrins, Part Two"; Lever, A. B. P., Gray, H. B., Eds.; Addison-Wesley: Reading, MA, 1983; pp 45–88.
(24) Taylor, C. P. S. *Biochim. Biophys. Acta* **1977**, *491*, 137–149.
(25) Scholes, C. P.; Lapidot, A.; Mascarenhas, R.; Inubushi, T.; Isaacson, R. A.; Feher, G. *J. Am. Chem. Soc.* **1982**, *104*, 2724–2735.
(26) Carrington, A.; McLachlan, A. D. "Introduction to Magnetic Resonance with Applications to Chemistry and Chemical Physics"; Harper and Row: New York, 1967; p 15.

$$\vec{\mu}_e = -\beta_e(g_x S_x \hat{i} + g_y S_y \hat{j} + g_z S_z \hat{k})$$

$$\vec{\mu}_n = \beta_n g_n (I_x \hat{i} + I_y \hat{j} + I_z \hat{k}) \quad (4)$$

where $\hat{i}$, $\hat{j}$, and $\hat{k}$ are unit vectors along the principal g_x, g_y, and g_z directions. An approximation which is useful in determining the first-order dipolar coupling, when the magnetic field is applied along a principal g axis (z perhaps) and the nuclear Zeeman interaction is also quantized along the same direction, is

$$A_{dip} = \frac{g_z \beta_e g_n \beta_n}{r^3} (3 \cos^2 \theta - 1) \quad (5)$$

If θ is substantially away from 0° or 90° turning points, then any misalignment of the magnetic field away from g_z will have a broadening effect on the dipolar interaction. Equation 5 is thus most useful in interpreting dipolar interactions and predicts well-resolved interactions when θ is near 0° or 90°.

When we are doing EPR-ENDOR at g values where the magnetic field orientations are off the principal axes, theoretical and experimental complications especially in dipolar-coupled proton ENDOR spectra can occur.[27] Anisotropic electron g values, like those here, make the axis of the electron spin quantization not in the direction of the applied magnetic field. Concomitantly, the nuclear Zeeman interaction may not commute with the dipolar interaction. Even so, it is possible, even likely, to obtain peaks in the ENDOR intensity from frozen solution when one is away from a principal g axis. At any particular off-axis g-value, there will be a spread of orientations which yield a distribution of ENDOR frequencies for a particular nucleus. There may, however, be a number of peaks in this distribution corresponding to orientations where the ENDOR frequency changes only slowly with the angle. In simpler Cu systems, such peaks in the powder ENDOR spectrum have been interpreted in a detailed, computerized fashion to ascertain proton coordinates.[27]

Results and Discussion

EPR Spectra and *g* Tensors. g values for the types of samples we studied are as follows: g_z, g_y, g_x = 2.92, 2.30, 1.56 [(TPP)Fe(Im)$_2^+$];[16] 2.96, 2.26, 1.52 [(OEP)Fe(Im)$_2^+$]; 2.82, 2.26, 1.68 [(COP)Fe(Im)$_2^+$]; 2.91, 2.26, 1.53 [MbIm]; 3.03, 2.23, 1.43 [cytochrome b_5];[14a] 3.03, 2.24, 1.24 [cytochrome a].[14a]

Because the structure of MbIm has been obtained from the Fourier difference study, we wanted to know if there was a relation between the g-tensor directions[11] and the coordinates and orientations of the heme plane and imidazole planes. The authors of ref 10 kindly provided their newly determined coordinates for the exogenous imidazole to us. We relied, as did the authors of ref 10, on older coordinates of the heme and proximal imidazole from Takano's X-ray determination of aquometmyoglobin.[28] We found that the g_z direction pointed within 9° of the normal to the heme plane, while g_x and g_y directions pointed within 10° of the meso carbons. g_y pointed in the direction of the meso carbon situated between the two pyrroles that have propionic groups. The plane of the exogenous imidazole (determined by its C_5–C_2 direction) was within 20° of the g_y direction, while the normal to the exogenous imidazole plane (determined by the normal to the C_5–N_1–C_2 plane) was within 24° of the g_x direction. The corresponding larger angles for the proximal imidazole were, respectively, 55° and 53°. So, if there is a correlation of the g_x and g_y directions with the π-bonding direction to an imidazole, the correlation is with the exogenous imidazole of MbIm, and it is g_x that is closest to the π-bonding direction normal to the exogenous imidazole plane.

Results—Nitrogen ENDOR. Our initial goal was simply to find characteristic, positively identifiable ENDOR signals from the imidazole nitrogen in low-spin ferric heme complexes. Since ^{15}N gives simpler two-line ENDOR patterns than ^{14}N and has a 40% larger nuclear magnetic moment, we were most successful in our initial work when we used ^{15}N-imidazole. Figure 2 here compares the nitrogen ENDOR spectra observed at g_y and g_x from MbIm having either [^{15}N]imidazole or [^{14}N]imidazole. A distinct peak, clearly from [^{15}N]imidazole, was observed in the 5–6-MHz region. The weak Zeeman partner to this peak was generally obscured in the [^{14}N]heme ENDOR, but by using a derivative presentation (inset in Figure 2), it was possible to enhance a weak Zeeman partner to it at about 3.1 MHz. Hence, the [^{15}N]imidazole peak clearly resolved in the 5–6-MHz region is the higher frequency Zeeman partner. As shown in Figure 4 of ref 29, the corresponding [^{15}N]imidazole ENDOR was also resolved in the 5–6-MHz region from the model (TPP)Fe(Im)$_2^+$ complex. The peak from [^{15}N]imidazole in (TPP)Fe(Im)$_2^+$ was broader and more intense than that from MbIm, possibly because there are two [^{15}N]imidazoles contributing from (TPP)Fe(Im)$_2^+$ but only one from MbIm. When the porphyrin contained naturally abundant ^{14}N while the imidazole contained ^{15}N, the ^{15}N peak in the 5–6-MHz region, as resolved at g_y or g_x, indicated imidazole (histidine) ligation and was used as an indicator of the histidine ligand in cytochrome a.[29]

ENDOR spectra obtained at g_z where the magnetic field is perpendicular to the heme have been useful in the past.[5] However, as shown in Figure 3, at g_z the ENDOR signals of both MbIm and (TPP)Fe(Im)$_2^+$ though distinct gave relatively little information on the imidazole ligand. In MbIm major peaks which we suspect to be [^{14}N]heme occurred at 4.70, 4.29, 3.10, and 2.89 MHz; in (TPP)Fe(Im)$_2^+$ the heme peaks occurred at 4.50 and 3.07 MHz. As shown in Figure 3b and d, there was at best a peak

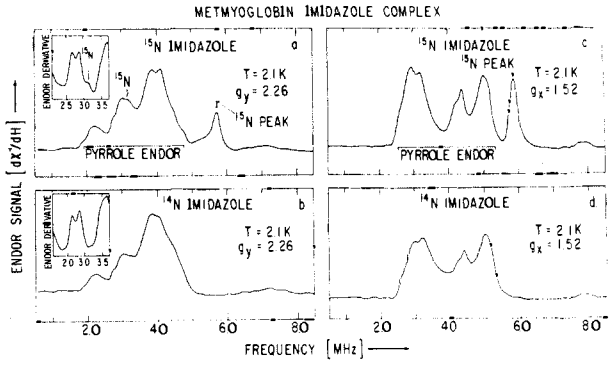

Figure 2. Comparison of nitrogen ENDOR from MbIm prepared either with [^{15}N]imidazole or [^{14}N]imidazole and observed at g_y and g_x. The ENDOR conditions are given in the Experimental Section. Each spectrum took about 20 min of signal averaging at a sweep rate of about 0.8 MHz/s. Spectra a and b were taken with a magnetic field of 2.87 kG. Spectra c and d were taken with a magnetic field of 4.28 kG. The insets to a and b are the derivative spectra over the given frequency region.

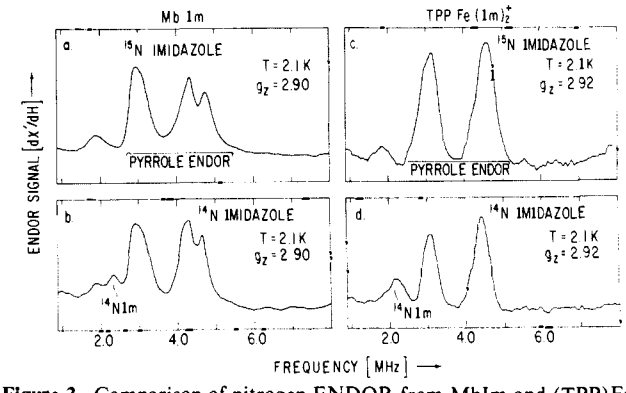

Figure 3. Comparison of nitrogen ENDOR from MbIm and (TPP)Fe(Im)$_2^+$ prepared either with [^{15}N]imidazole or [^{14}N]imidazole as observed at g_z. ENDOR conditions are given in the Experimental Section, and each spectrum took about 20 min of signal averaging at a sweep rate of about 0.8 MHz/s. The magnetic fields were about 2.24 kG.

(27) (a) Hurst, G. C. Ph.D. Thesis, University of Rochester, 1983. (b) Kreilick, R.; Henderson, T. A., private communication.
(28) Takano, T. *J. Mol. Biol.* **1977**, *110*, 537–568.
(29) Martin, C. T.; Scholes, C. P.; Chan, S. I. *J. Biol. Chem.* **1985**, *260*, 2857–2861.

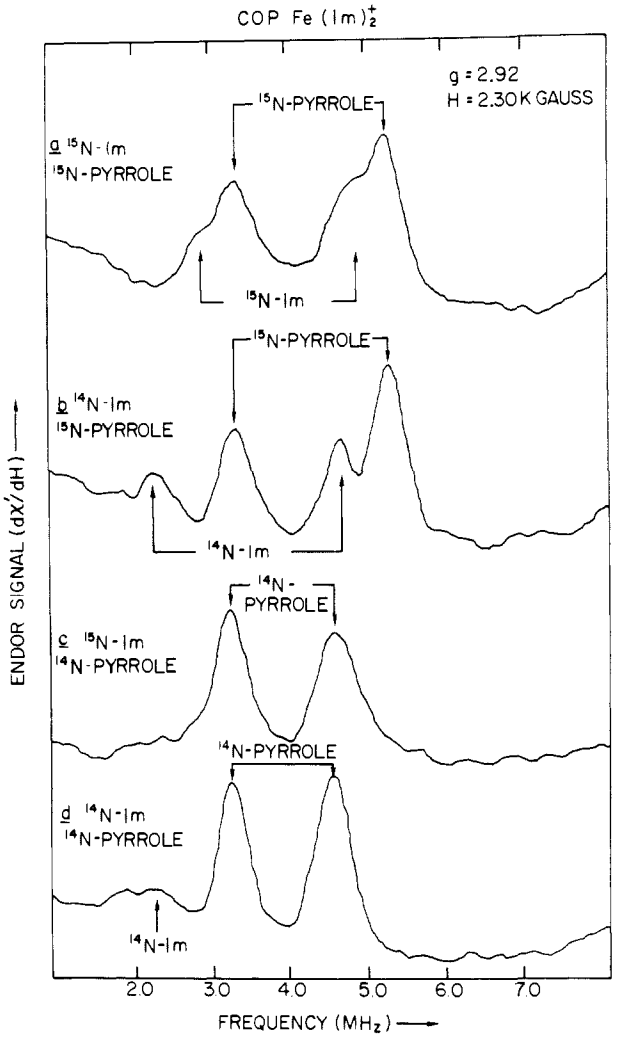

Figure 4. Comparison taken at $g = 2.92$ of nitrogen ENDOR from (COP)Fe(Im)$_2^+$ containing the four possible combinations of [^{15}N] or [^{14}N]pyrrole and imidazole. Each spectrum took about 20 min of signal averaging at a sweep rate of 0.8 MHz/s. The ^{15}N or ^{14}N peaks labeled here are features which can unambiguously be assigned to pyrrole or imidazole labeled by the appropriate isotope. The ^{15}N peaks are Zeeman partners (split by $2^{15}g_n\beta_nH$ = 1.98 MHz). The relation of the ^{14}N features to the specific terms in eq 2b is discussed in the text.

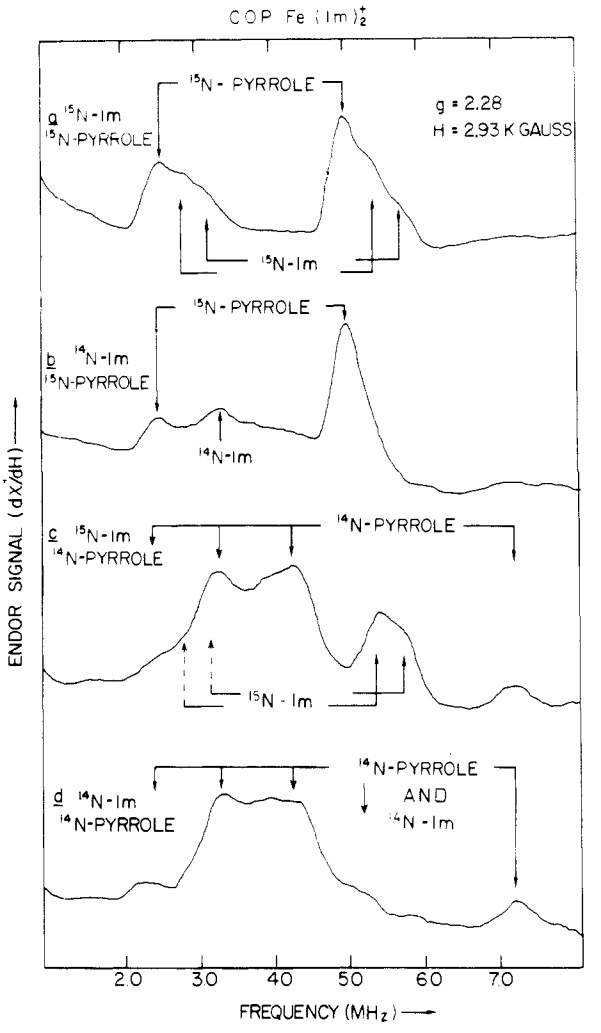

Figure 5. Comparison taken at a g value of 2.28 near g_y from (COP)-Fe(Im)$_2^+$ containing the four possible combinations of ^{15}N or ^{14}N on pyrrole and imidazole. In a and b, the ^{15}N features labeled with arrows are readily distinguished Zeeman partners split from each other by approximately $2^{15}g_n\beta_nH$ = 2.54 MHz. Features which are obviously from [^{14}N]imidazole and/or pyrrole are so labeled, but ^{14}N Zeeman partners are not readily distinguished. In c, the lower frequency [^{15}N]imidazole features near 3 MHz are not really resolved from under the ^{14}N features, but their expected position is indicated with dotted lines. In d, the feature at 5.0 MHz, which in a–c would have been hidden by ^{15}N ENDOR, appears; it is not obvious if it is from ^{14}N on imidazole or on pyrrole. The peak at about 7 MHz in c and d is from [^{14}N]pyrrole and is a $\Delta I = 2$ transition seen in other low-spin heme systems[5] and metal–nitrogen systems.[31] ENDOR conditions are as in Figure 4.

occurring at 2.2–2.3 MHz which could be traced to [^{14}N]-imidazole. A weak peak or shoulder occurred in many samples having [^{14}N]pyrrole at 1.7–1.8 MHz.

In all the foregoing ENDOR spectra from porphyrins with ^{14}N on the pyrroles, it was difficult to resolve detailed, interpretable spectral information from which one could extract hyperfine couplings and quadrupole couplings; both [^{15}N]- and [^{14}N]-imidazole peaks were largely obscured by [^{14}N]pyrrole, and the lower frequency Zeeman partner was often difficult to observe.[30] We were fortunate at this point to obtain the (COP)Fe(Im)$_2^+$ that had ^{15}N on the pyrrole nitrogens. Figures 4 and 5 show the ENDOR spectra of (COP)Fe(Im)$_2^+$ respectively obtained at g_z and g_y from (a) [^{15}N]imidazole, [^{15}N]pyrrole, (b) [^{14}N]imidazole, [^{15}N]pyrrole, (c) [^{15}N]imidazole, [^{14}N]pyrrole, and (d) [^{14}N]-pyrrole, [^{14}N]imidazole. This better ENDOR resolution of ^{15}N vs. ^{14}N was particularly obvious at g_y (Figure 5) where broadening of ENDOR features by the anisotropic quadrupolar interaction would hold for ^{14}N but not for ^{15}N. At g_y (Figure 5c and d), it is not really possible to identify ^{14}N Zeeman partners. Nevertheless, the selective use of ^{15}N on imidazole or on pyrrole does serve to reveal better some ^{14}N features at g_y. Detailed frequencies and assignments of peaks are given in Table I and in the figure legends to Figures 4 and 5. A comparison of [^{15}N]imidazole and [^{15}N]pyrrole ENDOR frequencies shows that at respective g values, the hyperfine couplings from these two types of nitrogen are fairly similar and isotropic. The ^{15}N hyperfine couplings and ENDOR frequencies for the imidazole nitrogen are somewhat less at g_z and greater at $g_{x,y}$ than for pyrrole nitrogen. The ENDOR spectra of the (COP)Fe(Im)$_2^+$ complexes with [^{14}N]pyrrole were similar to the spectra of the corresponding (TPP)Fe(Im)$_2^+$ com-

(30) It is generally the lower frequency member of a nitrogen nuclear Zeeman pair which has been harder to detect. Lower energy transitions arise from energy levels (see Figure 2, ref. 6) which are closer together, more nearly degenerate, and therefore more subject to broadening from second-order quadrupolar or hyperfine effects. This is particularly true when the nuclear Zeeman coupling ($g_n\beta_nH$) is of the same order as $A/2$. The rf-induced nuclear spin flip probability is thought to arise from two sources: first, direct coupling of the rf field with the nuclear magnetic moment and, second, rf modulation of the electron-nuclear hyperfine coupling (Davies, E. R.; Reddy, T. S. *Phys. Lett.* **1970**, *31A*, 398–399). The transition probability for a nuclear spin flip is proportional to the square of the sum of matrix elements for these two contributions. For one of the electron-spin manifolds in which ENDOR occurs (e.g., electron spin up), the two contributions will augment each other; in the other spin manifold, they subtract. Thus, some ENDOR transitions are more intense than others. In particular, if the two contributions subtract, the nuclear spin flip probability may be particularly small if the nuclear Zeeman coupling and the electron nuclear hyperfine coupling are comparable.

Table I

compd and conditions	ENDOR frequencies (MHz)[a] and assignments	derived first-order couplings, MHz
	A	
$(COP)Fe(1m)_2^+$	(Figure 4)	
$g_z = 2.92$	2.58 ± 0.06 $^{15}N_{1m}$	$\|^{15}A_{zz}\|_{1m} = 7.22 \pm 0.08$
$H = 2.30$ kG	4.64 ± 0.04 $^{15}N_{1m}$	
$2^{15}g_n\beta_nH = 1.98$ MHz	3.09 ± 0.02 ^{15}N-Pyr	$\|^{15}A_{zz}\|_{Pyr} = 8.16 \pm 0.03$
$2^{14}g_n\beta_nH = 1.41$ MHz	5.07 ± 0.02 ^{15}N-Pyr	
	2.09 ± 0.03 $^{14}N_{1m}$	$\|^{14}A_{zz}\|_{1m} = 5.12 \pm 0.04$
	4.44 ± 0.02 $^{14}N_{1m}$	$\|Q_{zz}\|_{1m} = 0.78 \pm 0.03$
	3.07 ± 0.02 ^{14}N-Pyr	$\|^{14}A_{zz}\|_{Pyr} = 6.07 \pm 0.03$
	4.41 ± 0.02 ^{14}N-Pyr	$\|Q_{zz}\|_{Pyr} = 0.45 \pm 0.02$
$(TPP)Fe(1m)_2^+$	(Figure 3c, d)	
	1.74 ± 0.05 ^{14}N-Pyr	
$g_z = 2.93$	2.16 ± 0.05 $^{14}N_{1m}$	
$H = 2.24$ kG	3.07 ± 0.04 ^{14}N-Pyr	$\|^{14}A_{zz}\|_{Pyr} = 6.18 \pm 0.06$
$2^{14}g_n\beta_nH = 1.38$ MHz	4.50 ± 0.04 ^{14}N-Pyr	$\|Q_{zz}\|_{Pyr} = 0.42 \pm 0.04$
MbIm	(Figure 3a, b)	
$g_z = 2.90$	1.85 ± 0.05 ^{14}N-Pyr	
$H = 2.24$ kG	2.30 ± 0.05 $^{14}N_{1m}$	
$2^{14}g_n\beta_nH = 1.38$ MHz		
	2.89 ± 0.02, 3.10 ± 0.02, 4.29 ± 0.03, 4.70 ± 0.03 ^{14}N-Pyr[b]	$\|^{14}A_{zz}\|_{Pyr} = 5.80, 6.42^b$ $\|Q_{zz}\|_{Pyr} = 0.46, 0.53^b$ $\|^{14}A_{zz}\| = 6.11, \|Q_{zz}\| = 0.50^b$ (av values for Pyr)
	B	
$(COP)Fe(Im)_2^+$	(Figure 5a–c)	
$g_y = 2.28$		
$H = 2.94$ kG	2.79 ± 0.03 $^{15}N_{1m}$[c]	
$2^{15}g_n\beta_nH = 2.54$ MHz	5.22 ± 0.03 $^{15}N_{1m}$	$\|^{15}A_y\|_{1m} = 8.01, 8.70$
	3.07 ± 0.03 $^{15}N_{1m}$[c]	$\|^{15}A_y\|_{1m} = 8.35$ (av)[c]
	5.63 ± 0.03 $^{15}N_{1m}$	
	2.34 ± 0.03 ^{15}N-Pyr	$\|^{15}A_y\|_{Pyr} = 7.18 \pm 0.05$
	4.84 ± 0.03 ^{15}N-Pyr	
$(TPP)Fe(Im)_2^+$	(Figure 4, ref 29)	
$g_y = 2.28$	5.43 ± 0.03 $^{15}N_{1m}$	
$H = 2.86$ kG	5.43 ± 0.03 $^{15}N_{1m}$	$\|^{15}A_y\|_{1m} = 8.37 \pm 0.06$
$2^{15}g_n\beta_nH = 2.47$ MHz	(upper Zeeman partner)	
MbIm	(Figure 2a)	
	3.14 ± 0.05 $^{15}N_{1m}$	$\|^{15}A_y\|_{1m} = 8.80 \pm 0.06$
$g_y = 2.26$	5.66 ± 0.02 $^{15}N_{1m}$	
$H = 2.87$ kG		
$2^{15}g_n\beta_nH = 2.49$ MHz		
	C	
$(COP)Fe(Im)_2^+$	5.30 ± 0.05 ^{15}N-Pyr	$\|^{15}A_x\|_{Pyr} = 6.86 \pm 0.10$
$g_x = 1.56$	(upper Zeeman partner)[d]	
$H = 4.33$ kG		$\|^{15}A_x\|_{1m} = 7.76 \pm 0.10$
$2^{15}g_n\beta_nH = 3.74$ MHz	5.75 ± 0.05 $^{15}N_{1m}$	
$(TPP)Fe(1m)_2^+$	5.59 ± 0.04 $^{15}N_{1m}$[c]	
$g_x = 1.54$		$\|^{15}A_x\|_{1m} = 7.53, 8.01^c$
$H = 4.24$ kG	(upper Zeeman partner)[d]	
$2^{15}g_n\beta_nH = 3.65$ MHz	5.83 ± 0.02 $^{15}N_{1m}$[c]	$\|^{15}A_x\|_{1m} = 7.77$ (av)[c]
MbIm	(Figure 2c)	
$g_x = 1.52$	5.84 ± 0.02 N_{1m}	$\|^{15}A_x\|_{1m} = 7.99 \pm 0.04$
$H = 4.28$ kG		
$2^{15}g_n\beta_nH = 3.69$ MHz	(upper Zeeman partner)[d]	

[a] Uncertainties in frequencies estimated from noise-related uncertainty in peak position. [b] ENDOR of inequivalent pyrrole ^{14}N's in MbIm yields separate estimates of ^{14}N hyperfine and quadrupole couplings. Average values from these separate estimates also given. [c] Two sets of inequivalent [^{15}N]imidazole were observed from several of the model bis(imidazole) porphyrins at g_y or g_x. The ^{15}N hyperfine couplings of these separate features are given as well as their average values. [d] In a number of cases the lower frequency ^{15}N Zeeman partner was weak or obscure. The hyperfine coupling was estimated from the observed Zeeman partner.

plexes. It did seem (see Figure 5 a and c) that there was some splitting of the [^{15}N]imidazole peak as resolved at g_y, but the average (center) frequency of this peak was approximately that observed from $(TPP)Fe(Im)_2^+$.

Nitrogen ENDOR—Discussion. The combination of data from all the various [^{15}N]imidazole complexes in Figures 2–5 and Table I shows that the imidazole ^{15}N hyperfine couplings found at $g_{z,y,x}$ are, respectively, in the range $|^{15}A_{zz}|_{1m} = 7.2$, $|^{15}A_y|_{1m} = 8.0$–8.8, and $|^{15}A_x|_{1m} = 7.5$–8.0 MHz. The couplings are undoubtedly from the Fe-liganding N-1 imidazole nitrogen because electron spin echo experiments have shown a much smaller coupling to more distant nitrogen (N-3) in metal complexes.[32] The hyperfine coupling in bis([^{15}N]imidazole) models showed more breadth and evidence for splitting of [^{15}N]imidazole ENDOR features (Figure 5a and 5c) beyond that in MbIm, which has only one [^{15}N]-imidazole. We have labeled the hyperfine couplings measured at g_y and g_x as A_y and A_x, rather than A_{yy} and A_{xx}; it may be that

(31) Rudin, M.; Schweiger, A.; Günthard, Hs. H. *Mol. Phys.* **1982**, *46*, 1027–1044.

(32) Peisach, J.; Mims, W. B.; Davis, J. L. *J. Biol. Chem.* **1979**, *254*, 12379–12389.

neither A_y or A_x is a principal hyperfine coupling because g_x and g_y axes may not be along principal hyperfine axes. Plausibly the splitting or breadth of the ENDOR signal from [^{15}N]imidazole in model porphyrins may derive from non-coincident g and A tensors. The hyperfine coupling to the *imidazole nitrogen* is still substantially isotropic with an average value [$^1/_3(|^{15}A_x|_{Im} + |^{15}A_y|_{Im} + |^{15}A_{zz}|_{Im})$] of 7.8 MHz. The hyperfine coupling at g_z, along or near the Fe–N-1 bond, is less than the coupling perpendicular to it by about 1.0 MHz; this is in contrast to the hyperfine coupling to the proximal imidazole in high-spin ferric metmyoglobin where the hyperfine coupling was larger along the Fe–N bond by about 3.5 MHz. In low-spin ferric heme systems, the unpaired electron spin is in a molecular orbital composed of metal d–π and p–π orbitals on the porphyrin and imidazole. There should be relatively little direct valence nitrogen 2s character of the unpaired electron spin. If there is a substantial isotropic contact interaction at the nitrogen, it must arise from exchange polarization of nitrogen s orbitals.[31] In low-spin Fe-liganded $^{13}CN^-$ complexes, including heme, such an exchange mechanism puts negative spin density on the $^{13}CN^-$.[33,34] If a similar mechanism involving exchange polarization and negative spin density accounts for the contact interaction at the Fe-liganded nitrogen of imidazole and heme, then the sign of the hyperfine coupling (which is not easily measured by ENDOR) is positive for ^{15}N and negative for ^{14}N. For the imidazole, the dipolar interaction of the electron spin on the nearby Fe would subtract from the contact interaction when the magnetic field was along the Fe–N-1 bond and add to the contact interaction when the magnetic field was perpendicular to the Fe–N-1 bond of imidazole. Hence, $|^{15}A_{zz}|_{Im}$ should be smaller than $|^{15}A_x|_{Im}$ or $|^{15}A_y|_{Im}$. In the high-spin ferric case, direct transfer of the electron spin from metal d_z^2 to nitrogen σ orbitals accounts for *positive* spin density in the nitrogen 2s valence orbitals. The latter situation makes the contact interaction and dipolar interaction augment each other when the magnetic field is along the Fe–N-1 bond and subtract from each other when the magnetic field is perpendicular to the Fe–N-1 bond.

With ^{15}N hyperfine couplings in hand, we could work backwards from observed [^{14}N]imidazole ENDOR features in (COP)Fe(Im)$_2^+$ (Figure 4 c, d) to obtain a value for $|^{14}A_{zz}|_{Im}$ in good agreement with the known ratio of ^{15}N and ^{14}N nuclear g values. The observed [^{14}N]imidazole ENDOR frequencies correspond to the expressions of eq 4b with $\nu_{ENDOR} = {}^1/_2|^{14}A_{zz}| \pm {}^3/_2|Q_{zz}| + {}^{14}g_n\beta_nH$, while weak and obscured values correspond to ${}^1/_2|^{14}A_{zz}| \pm {}^3/_2|Q_{zz}| - {}^{14}g_n\beta_nH$. We obtained an imidazole N-1 quadrupole coupling, $|Q_{zz}|$, of about 0.8 MHz in magnitude. This quadrupole coupling is significantly less in magnitude than the quadrupole coupling measured along the Fe–N bond in high-spin aquometmyoglobin ($|Q_{zz}| = 1.12$). In low-spin ferric heme systems, there is no covalent electron spin population in the d_z^2 orbital. In the high-spin ferric system, the d_z^2 orbital is populated with unpaired spin and is directed for σ bonding at the axial imidazole. Thus, there should be less electron density in the imidazole σ orbital directed toward the metal in low-spin ferric heme systems. Using the Townes–Dailey treatment outlined in eq 11 of ref 25, one finds that this lack of pσ density lowers the magnitude of Q_{zz} (making Q_{zz} less negative) in low-spin ferric heme imidazole complexes.

The [^{15}N]pyrrole nitrogen couplings were similar in magnitude to those observed elsewhere for low-spin pyrrole nitrogens[5], but because of our use of various permutations of ^{15}N and ^{14}N isotopes, the set of couplings measured here for [^{15}N]pyrrole nitrogen is the most complete set. The isotropic coupling measured from [^{15}N]pyrrole in (COP)Fe(Im)$_2^+$ is 7.4 MHz. As with [^{14}N]-imidazole, one finds that the more intense peaks at g_z observed from [^{14}N]pyrrole must correspond to $\nu_{ENDOR} = {}^1/_2|^{14}A_{zz}| \pm {}^3/_2|Q_{zz}| + {}^{14}g_n\beta_nH$ in eq 2b. The resultant values of hyperfine, $|^{14}A_{zz}|_{Pyr}$, and quadrupole, $|Q_{zz}|_{Pyr}$, couplings for (TPP)Fe(Im)$_2^+$ and (COP)Fe(Im)$_2^+$ are 6.07 and 0.45 MHz, respectively.

The reader may note that the first-order hyperfine couplings $|A_{zz}|_{Pyr}$ for ^{15}N and ^{14}N in Table IA are, respectively, 8.16 ± 0.03 and 6.07 ± 0.03 MHz. If the ^{15}N measurement is correct, then one can predict from the magnetic moments of ^{15}N and ^{14}N ($^{15}g_n = -0.566$; $^{14}g_n = 0.403$) that the ^{14}N hyperfine coupling should be 5.81 MHz. We maintain that this discrepancy is not due to error in the data. Rather, it is due to the need for a second-order quadrupolar correction to the first-order ENDOR expressions of eq 2b, from which the first-order estimates of ^{14}N hyperfine couplings in Table IA were derived. We have previously observed the need for such a correction in our single-crystal ENDOR work on the heme nitrogens of aquometmyoglobin, we have derived formulas for it there, and we have discussed it in detail. (See ref 25, p 2730.) This correction is approximately $(Q_{xx} - Q_{yy})^2/(2|^{14}A_{zz}|)$. We have not yet determined Q_{xx} and Q_{yy} for low-spin ferric pyrrole nitrogen, but since these quadrupolar couplings depend on the overall electronic population at the nitrogen, rather than just the unpaired spin, the values of Q_{xx} and Q_{yy} are probably in reasonable agreement with the values from high-spin ferric heme which are known to be $Q_{xx} = -0.77$ and $Q_{yy} = 1.04$ MHz.[25] If we take $|^{14}A_{zz}|_{Pyr} = 6.07$ MHz, we compute a correction to be subtracted from the first-order estimate of 6.07 MHz of 0.26 MHz. Thus, the actual hyperfine coupling for $|^{14}A_{zz}|_{Pyr}$ would be 5.81 MHz, a number no longer in disagreement with the value of $|^{15}A_{zz}|_{Pyr}$. For imidazole, the values of Q_{xx} and Q_{yy} were much closer to each other in magnitude and of the same sign,[25] so the correction for the imidazole's first-order ^{14}N hyperfine coupling turns out to be only about 0.02 MHz. Thus, the imidazole ^{15}N and ^{14}N hyperfine couplings are in good agreement without need for the quadrupolar correction.

In MbIm, as in other low-spin myoglobin complexes,[5] there is a splitting of the heme nitrogen ENDOR peaks, and this implies differing electron densities on various heme nitrogens. (In ref 5, this splitting was identified as truly at the pyrrole nitrogens through the use of a special hemoglobin which had 50% ^{15}N isotopic substitution on the pyrroles.) The hyperfine couplings differ between inequivalent nitrogens of pyrrole in MbIm by about 10%. We note that in high-spin aquometmyoglobin, a 5% difference in hyperfine couplings was found between diagonally opposite pyrrole nitrogens.[25]

Weakly Coupled Porphyrin Proton ENDOR—Results. Porphyrin protons typically have hyperfine couplings less than 2 MHz in magnitude.[5] Spectra a and b in Figure 6, respectively, show the ENDOR signals from pyrrole protons (of D-20 TPP) and phenyl protons (of D-8 TPP) measured at the g_z maximal g value known to be perpendicular to the heme. The summed signals from the pyrrole protons in Figure 6a and phenyl protons in Figure 6b yielded a net signal (Figure 6d) very similar to that from fully protonated TPP (Figure 6c). From TPP's D_{4h} symmetry, one might expect the spin density at each pyrrole proton to be the same, so when the magnetic field was along the heme normal (i.e., along the porphyrin's 4-fold axis), these protons could be magnetically and electronically equivalent. However, there were dual sets of pyrrole proton ENDOR peaks, one set with a hyperfine coupling of about 1.0 MHz and the other set with a larger coupling of about 1.7 MHz. The relative intensity and frequency of hyperfine coupling for these two pyrrole proton sets did not change as we went to lower magnetic fields and higher g values at the low field extreme of the g_z signal; such change might occur if there were slightly different (TPP)Fe(Im)$_2^+$ complexes having different g values and different electronic structures. Rather, it must be that the ENDOR technique is showing that pyrrole protons on the same TPP have different hyperfine couplings. It would be convenient if each TPP had four pyrrole protons contributing to the ENDOR features with 1.7-MHz coupling and four pyrrole protons contributing to the ENDOR features with 1.0-MHz coupling. However, the explanation for ENDOR intensities in solids is sufficiently complex[6] that we cannot be sure if the same number of protons contribute to each of the respective features. The overall hyperfine couplings to phenyl protons are smaller than for the pyrrole protons, and there may be some overlap of ortho, meta, and para proton resonances. So far as we can tell, there is no additional splitting of phenyl proton features beyond that expected for ortho, meta, and para inequivalence.

(33) Goff, H. J. *J. Am. Chem. Soc.* **1977**, *99*, 7723–7724.
(34) Kuska, H. A.; Rogers, M. T. *J. Chem. Phys.* **1964**, *41*, 3802–3805.

Table II. Proton Hyperfine Interactions Computed from NMR Contact Information, Compared with ENDOR Data. Proton Hyperfine Coupling $|A_{zz}| = |A_{dip} + A_{contact}|$; $A_{dip} = g_z\beta_e g_n\beta_n/r^3\ (3\cos^2\theta - 1)$; $g_z = 2.91$

compound	position	$(3\cos^2\theta - 1)/r^3$, Å^{-3}	A_{dip}, MHz	$A_{contact}$, MHz	$\|A_{zz}\|$(computed), MHz	$\|A_{zz}\|$(ENDOR), MHz
$(TPP)Fe(Im)_2^+$	ortho-H	−0.003 63[a,b]	−0.42[b]	0[a]	0.42	0.57 ± 0.03
$(TPP)Fe(Im)_2^+$	meta-H	−0.001 65[a,b]	−0.19[b]	0[a]	0.19	0.23 ± 0.03
$(TPP)Fe(Im)_2^+$	para-H	−0.001 48[a]	−0.17	0[a]	0.17	0.23 ± 0.03
$(TPP)Fe(Im)_2^+$	pyrrole-H	−0.006 83[a]	−0.78	−0.67[a]	1.45	1.71 ± 0.03[c]
						0.96 ± 0.03[c]
$(OEP)Fe(Im)_2^+$	meso-H	−0.010 8[a]	−1.24	+0.08[a]	1.16	1.11 ± 0.03
MbIm	meso-H					1.08 ± 0.03
cyto b_5	meso-H					1.05 ± 0.03
cyto *a*	meso-H					1.05 ± 0.03
OEP	pyrrole-CH_2	−0.005 69[a]	−0.65	+0.18[a]	0.47	0.48 ± 0.03

[a] Reference 7. [b] Because phenyl groups are found rotated in the crystal, these are average values for ortho- and meta-phenyl protons. We find that the dipolar coupling computed from X-ray data (ref 8) varies for ortho from 0.54 to 0.19 MHz and for meta from 0.22 to 0.11 MHz. [c] As noted in text, the pyrrole protons show strong evidence for inequivalence.

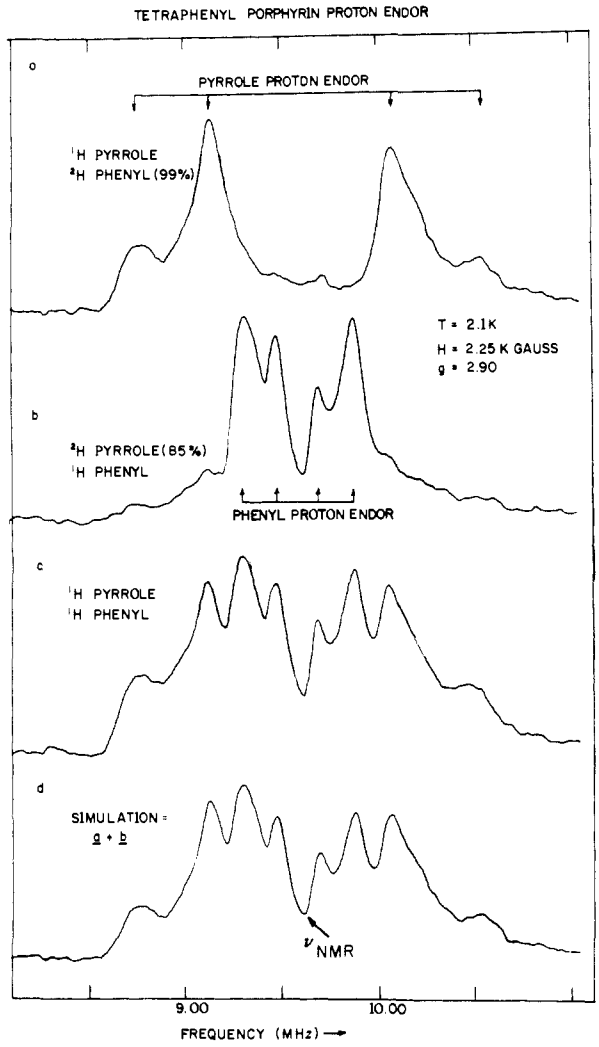

Figure 6. Weakly coupled proton ENDOR spectra from pyrrole and phenyl protons of $(TPP)Fe(Im)_2^+$ dissolved in deuterated $CDCl_3$ and CD_2Cl_2 and prepared with fully deuterated imidazole. All spectra were taken near the g_z extremum and under conditions described in the Experimental Section; a small field modulation of 0.20 G p.t.p. was used: (a) from $(TPP)Fe(Im)_2^+$ prepared with D-20 (99%) TPP; (b) from $(TPP)Fe(Im)_2^+$ prepared with D-8 (85%) TPP; (c) from $(TPP)Fe(Im)_2^+$ prepared with fully protonated TPP; (d) sum of a + b and is offered to compare with c.

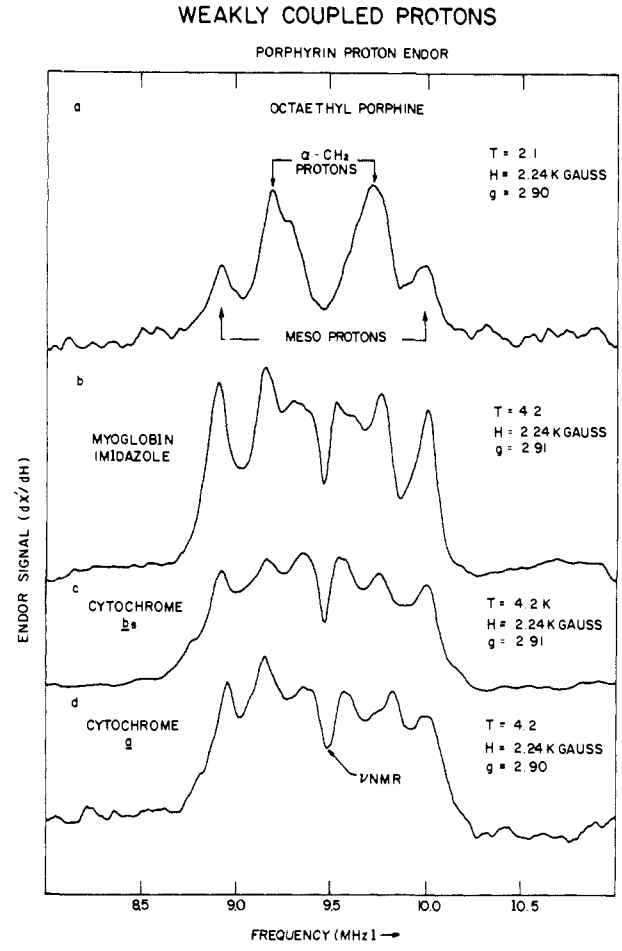

Figure 7. Weakly coupled proton ENDOR spectra from porphyrin systems that have meso protons. All spectra were taken near the g_z extremum and taken under conditions described in the Experimental Section; a small field modulation of 0.20 G p.t.p. was used. (a) from $(OEP)Fe(Im)_2^+$ dissolved in $CDCl_3$–CD_2Cl_2 and prepared with fully deuterated imidazole; (b) from MbIm in deuterated buffer and prepared with deuterated imidazole; (c) from cytochrome b_5 in protonated buffer; (d) from cytochrome *a* in protonated buffer. The spectra c and d sharpened somewhat if they were taken at a *g* value of 3.00.

The naturally occurring porphyrins, and OEP as well, have meso protons rather than phenyl groups. When we performed ENDOR (Figure 7a) on the protons of $(OEP)Fe(Im)_2^+$, we noted proton ENDOR peaks not seen from TPP complexes, and as discussed below, the coupling of these protons was close to that predicted for meso protons. Unlike the pyrrole protons, no splitting of ENDOR features from the meso protons, which ought to have equivalent electron densities under the OEP's formally D_{4h} symmetry, was noted. Thus, the meso protons do appear to be electronically equivalent. In OEP, the ENDOR signals that must have come from the α-CH_2 protons on the outer pyrrole carbons were sufficiently overlapping in hyperfine coupling that we could not directly resolve from them an inequivalence of electron density at pyrrole carbons. MbIm, cytochrome b_5, and cytochrome *a* all

showed proton ENDOR peaks with about the same splitting as that observed for the meso protons of $(OEP)Fe(Im)_2^+$. Detailed couplings and ENDOR frequencies are given in Table II.

Weakly Coupled Porphyrin Protons—Discussion. From X-ray coordinates[8] and a carbon–proton bond distance of 1.08 Å, the distances and angles to various relevant porphyrin protons could be determined. As shown in the third and fourth columns of Table II, values of $(3\cos^2\theta - 1)/r^3$ and of the dipolar coupling were calculated. The latter values were computed from eq 5 where $g_z = 2.91$ was taken to point normal to the heme plane. Some of these same numbers were computed by the authors of ref 7 and 9, and our numbers are in agreement with theirs. We point out that the respective computed dipolar couplings in Table II for ortho and meta phenyl protons are average values for the specific type of proton because the four phenyl planes in the crystallographic structure[8] showed different rotations with respect to the porphyrin plane. On the other hand, the respective computed dipolar couplings for all outer pyrrole protons (−0.78 MHz) and all meso protons (−1.24 MHz) were identical because these protons attach rigidly to the porphyrin plane. The absolute values of the contact plus computed dipolar contributions (sixth column, Table II) gave numbers whose magnitudes agreed with the respective magnitudes of proton ENDOR couplings (seventh column, Table II). For $(TPP)Fe(Im)_2^+$, the average of the two ENDOR-determined pyrrole proton couplings (1.35 MHz average) was close to the predicted 1.45-MHz value for pyrrole protons.

Our experiments unambiguously showed magnetic inequivalence of outer pyrrole protons, and it is important to explain this inequivalence and the implications that it has for the electronic structure of low-spin ferric heme. It is extremely unlikely that the approximate 0.7-MHz inequivalence between pyrrole protons would be caused by inequivalence of the dipolar interaction, whose entire magnitude is only slightly greater than the inequivalence itself. Rather, the inequivalence of pyrrole proton hyperfine couplings must be due to a distribution of π-electron spin over the porphyrin periphery which results in different contact interactions at different pyrrole protons. It is known from previous NMR work that the pyrrole protons of $(TPP)Fe(Im)_2^+$ have a substantial contact interaction (fourth column, Table II) that reflects the electron spin density on their adjacent carbons, while meso protons and meso phenyl groups have very small contact interactions, reflecting little unpaired spin density on meso carbons. Commonly used empirical (McConnell) relations[35] indicate that an α proton will experience −0.7 MHz of contact interaction for each 1% of unpaired electron on its adjacent α carbon. Once the computed dipolar interaction is removed, the ENDOR results here from $(TPP)Fe(Im)_2^+$ yielded contact interactions for the two inequivalent types of pyrrole protons that are about −0.2 and −0.9 MHz. Thus, the two types of pyrrole protons differ in unpaired π-electron density at their α carbons by a factor of about 4.5, and differ in α-carbon electron spin density by about 1%. The overall unpaired electron density delocalized out to the pyrrole periphery will be less than 10% of an unpaired electron, so most of the unpaired electron density will reside closer to the heme iron.

It is of interest to know if such inequivalence of pyrrole protons has been previously observed from $(TPP)Fe(Im)_2^+$ complexes. The previous high-resolution solution NMR carried out on $(TPP)Fe(Im)_2^+$ complexes made with standard imidazole has obtained an average hyperfine coupling to the pyrrole protons.[7,9] Rapid reorientation of magnetic axes on the NMR time scale is thought to average out the inequivalence between pyrrole protons. However, more recent NMR work has been carried out on specially modified porphyrins, including TPP's, which have long side chains designed to restrict the orientation of the imidazole ligand simply by the physical bulk of the side chain or by actual attachment to an imidazole.[3a,c] In these systems, there is measurable inequivalence of pyrrole proton contact interactions. In our system, it appears that a conformation of TPP and its imidazole ligands is frozen in at low temperatures, and this conformation gives rise to the rhombic splitting of the d_{xz}, d_{yz} orbitals, to the g_x, g_y anisotropy, and to the inequivalence in pyrrole hyperfine couplings. Since all the bis(imidazole) systems, both protein and model, studied here have very similar rhombic splittings and g values, it is tempting to say that the nature of the perturbation on the symmetry is the same for all these systems. Plausibly this perturbation involves a specific orientation of axial imidazoles for minimum steric repulsion by pyrrole nitrogens and/or a natural tendency of the porphyrin, abetted by its imidazole ligands, to distort so as to remove d_{xz}–d_{yz} degeneracy.

The magnetic inequivalence of pyrrole protons could arise when the degeneracy of the metal d_{xz} and d_{yz} orbitals is removed and the resultant inequivalent and unequally populated d_{xz} and d_{yz} orbitals are coupled into porphyrin orbitals of the proper symmetry. NMR workers have interpreted contact interactions at pyrrole positions in low-spin ferric heme as arising from covalent coupling of the filled E_g porphyrin orbitals into the metal d_{xz} and d_{yz} orbitals. Such E_g orbitals which can be obtained from early molecular orbital computations[36] are observed to have much electron density on pyrrole carbons but very little on meso carbons.[3c] If we take the convention of the d_{yz} orbital having the most unpaired spin, then the E_g orbital that couples into the d_{yz} orbital will have more unpaired electron spin than the E_g orbital that couples into the d_{xz} orbital. There will thus be different contact couplings for different pyrrole carbons. Ab initio one does not know where the x and y axes should point with respect to pyrrole nitrogens. One potentially interesting direction for x and y axes would be at 45° to the heme nitrogen diagonals. As indicated in ref 3c, such a 45° orientation would leave those outer pyrrole protons nearer the x axis with about $^1/_3$ of the electron spin density on their adjacent carbons of the pyrrole protons closer to the y axis. This 45° orientation would be consistent with determination of the x, y axes by an imidazole plane that makes 45° angles to the pyrrole nitrogen diagonals. Such a 45° orientation would also leave the π-electron density at all four pyrrole nitrogens the same.

Imidazole Protons—Results. Spectra of $(TPP)Fe(Im)_2^+$ complexes (Figure 8) showed ENDOR from protons whose couplings are greater than those of the porphyrin. The source of such protons is the imidazole. The ENDOR of $(TPP)Fe(Im)_2^+$ with selectively deuterated (Figure 1, **6c**, **6d**) imidazoles strongly implicated the C-2 and C-5 protons of imidazole, hereafter called H-2 and H-5. Selectively deuterated imidazoles also reduced the number of overlapping proton ENDOR transitions. The intensity of these upper and lower Zeeman pairs belonging to a particular proton was characteristically unequal. The ENDOR spectra of imidazole protons were extensively followed at numerous g values from g_z to g_x and markedly changed as a function of g value. The best resolution of the most features was in the $g = 2.4$–2.5 region rather than at g-value extrema. The frequencies and assignments of the imidazole protons obtained at these 2.4–2.5 g-values are given in Table III. Peaks 2 and 2′ (from H-2) and 5a and 5a′ (from H-5), whose splittings away from the free proton frequencies were respectively ±1.9 and ±1.6 MHz, were resolved over a wide g-value range from $g = 2.5$ to $g < 2.0$. The largest obtainable splitting anywhere of ±2.65 MHz away from the free proton frequency occurred at $g = 2.58$ and was from H-5. The corresponding largest splitting for H-2 was ±2.1 MHz at $g = 2.58$. The resolution of ENDOR from imidazole protons was poor at g_z, but at g_x (Figure 9), couplings of 1.8 and 2.6 MHz were resolved and assigned to H-5 and H-2, respectively. We did find an outlying H-2 feature with a coupling of 2.6 MHz from the ENDOR of MbIm at g_x, and this feature lost intensity when the H-2 proton of the exogenous imidazole was replaced by deuterium through the use of selectively deuterated imidazole (Figure 1, **6d**). Unfortunately, the more weakly coupled H-5 proton was obscured by overlap with other proton signals.

Figure 10 shows spectra from bis(imidazole) proteins similar to, but not identical with, the spectra of $(TPP)Fe(Im)_2^+$ made

(35) Wertz, J. E.; Bolton, J. R. "Electron Spin Resonance, Elementary Theory and Practical Applications"; McGraw-Hill: New York, 1972; Chapter 5, pp 97–98.

(36) Longuet-Higgins, H. C.; Rector, C. W.; Platt, J. R. *J. Chem. Phys.* **1950**, *18*, 1174–1181.

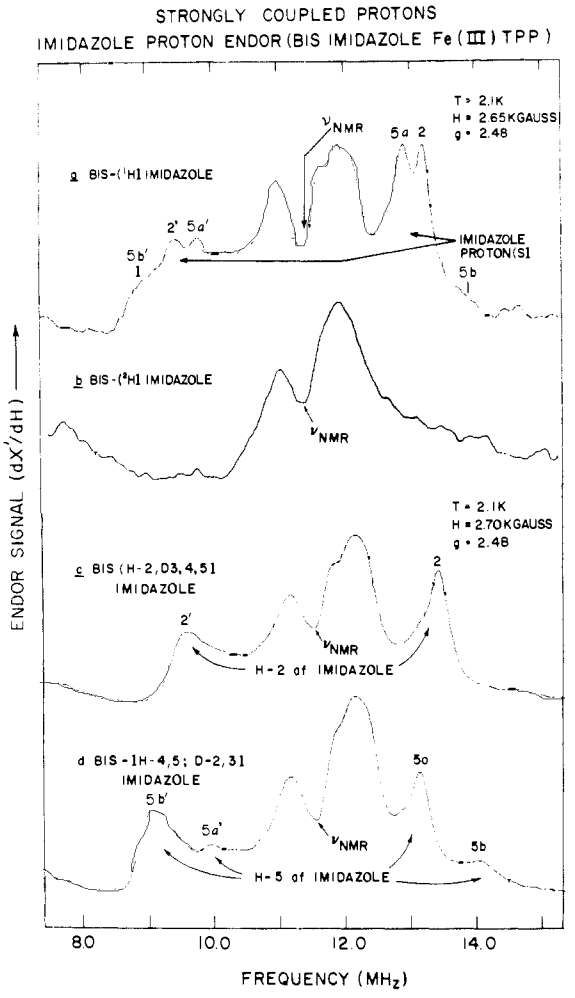

Figure 8. Comparison of proton ENDOR from $(TPP)Fe(Im)_2^+$ complexes prepared with various deuterated and protonated imidazoles. The emphasis is on strongly coupled protons of the imidazole. The proton ENDOR from these was best brought in with a 100-kHz field modulation of 0.8 G p.t.p. and a frequency sweep rate of 0.8 MHz/s. The electronic g value was 2.48. Each spectrum took about 10 min of signal averaging: (a) ENDOR from strongly coupled protons of $(TPP)Fe(Im)_2^+$ prepared with fully protonated imidazole in deuterated $CDCl_3$–CD_2Cl_2 solvent; (b) ENDOR from $(TPP)Fe(Im)_2^+$ prepared with fully deuterated imidazole in $CDCl_3$–CD_2Cl_2 (note lack of strongly coupled protons; weakly coupled protons are from the porphyrin); (c) ENDOR from strongly coupled protons of $(TPP)Fe(Im)_2^+$ prepared with imidazole protonated only at H-2 (the proton ENDOR features are thus labeled 2 and 2'); (d) ENDOR from strongly coupled protons of $(TPP)Fe(Im)_2^+$ prepared with imidazole protonated on H-4 and H-5. (because of H-5's much closer proximity to Fe and known magnitude of contact interaction, the peaks are assigned to H-5 rather than H-4; the Zeeman pairs are labeled 5a, 5a' and 5b, 5b').

from fully protonated imidazole. As with $(TPP)Fe(Im)_2^+$ made with the fully protonated imidazole, some of the imidazole proton peaks were obscured; however, common features in Figure 10 labeled [in analogy with $(TPP)Fe(Im)_2^+$ complexes] 2, 5a, and 5b were consistently found, and their frequencies are given in Table III. The outlying peak labeled 5b, which was due in $Fe(TPP)(Im)_2^+$ to H-5, has a neighbor labeled c' in cytochrome b_5 and a. The MbIm prepared with fully deuterated exogenous imidazole, but still having protonated proximal imidazole, showed an approximate 50% reduced intensity of its outlying imidazole proton features; the implication is that in the $g = 2.4$ region both exogenous and endogenous imidazoles of MbIm contributed to the ENDOR features, and both yielded approximately the same ENDOR frequency. The proteins MbN_3^- and cytochrome c, which lack bis(imidazole) coordination, did not show the characteristic well-resolved spectra like those of Figure 10.

We wanted to discern couplings to more distant protons of imidazole, notably to the exchangeable proton (H-3) on the N-3.

Table III. ENDOR of Strongly Coupled Imidazole Protons

complex	peak[a]	difference (MHz) of peak freq and ν_{NMR}	first-order hyperfine coupling, MHz	assignment
$(TPP)Fe(Im)_2^+$	2	1.85 ± 0.02	3.75 ± 0.06	(H-2)
at $g = 2.48$	2'	−1.90 ± 0.05		
Figure 8	5a	1.56 ± 0.02	3.16 ± 0.06	(H-5)
	5a'	−1.60 ± 0.04		
	5b	2.42 ± 0.04	4.82 ± 0.06	(H-5)
	5b'	−2.40 ± 0.04		
MbIm	2	1.76 ± 0.02	3.52 ± 0.04[b]	(H-2)
at $g = 2.42$,	5a	1.36 ± 0.02	2.72 ± 0.04[b]	(H-5)
Figure 10a	5b	2.34 ± 0.04	4.68 ± 0.07[b]	(H-5)
	5b'	2.34 ± 0.06		
cytochrome b_5	2	1.81 ± 0.02	3.62 ± 0.04[b]	(H-2)
at $g = 2.42$,	5a	1.54 ± 0.02	3.08 ± 0.04[b]	(H-5)
Figure 10b	5b	2.63 ± 0.06	5.32 ± 0.10	(H-5)
	5b'	−2.69 ± 0.06		
	c'	−2.02 ± 0.06	4.04 ± 0.12[b,c]	
cytochrome a	2	1.85 ± 0.02	3.70 ± 0.04[b]	(H-2)
at $g = 2.42$,	5a	1.46 ± 0.02	2.92 ± 0.04[b]	(H-5)
Figure 10c	5b	2.36 ± 0.10	4.72 ± 0.12	(H-5)
	5b'	−2.36 ± 0.06		
	c'	−1.98 ± 0.06	3.96 ± 0.12[b,c]	

[a] Features are labeled according to the imidazole proton to which they are assigned, based on work with selectively deuterated imidazole complexes of TPP. The unprimed features are those above ν_{NMR}, and the primed features are below ν_{NMR}. [b] In proteins, one Zeeman partner is sometimes obscured so that hyperfine couplings have been computed from only one proton ENDOR feature. [c] The feature c' only occurs in cytochrome a and b_5; it appears to be imidazole in origin, but we are not sure of which proton.

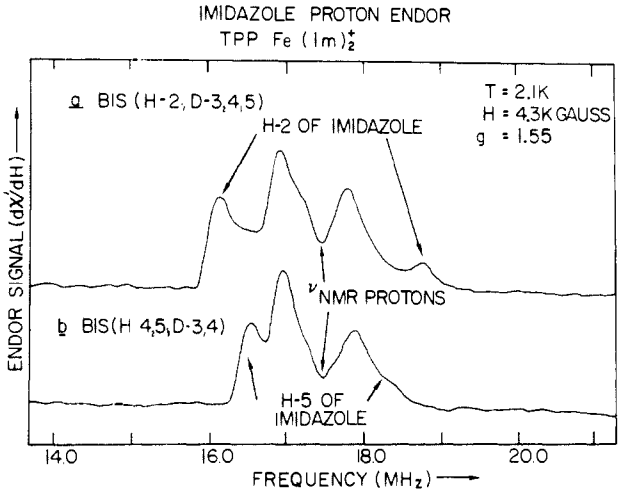

Figure 9. Comparison of proton ENDOR obtained from $(TPP)Fe(Im)_2^+$ prepared either with imidazole protonated only on H-2 or with imidazole protonated on H-4 and H-5. Conditions used are similar to those of Figure 8. The g value, however, was the extremal value of g_x: (a) ENDOR from the strongly coupled H-2 proton; (b) ENDOR from the strongly coupled H-5 proton.

The clearest of such couplings came from MbIm and was best resolved at g_y, where the exchangeable proton hyperfine coupling was 1.2 MHz. Figure 11 shows a comparison of spectra from MbIm taken in protonated and deuterated buffer. In both cases, the carbons of the exogenous imidazole were fully protonated, but similar spectra were observed from deuterated imidazole. When we used *N*-methylimidazole (Figure 1, **6f**), the exchangeable, imidazole-related proton was no longer observed by ENDOR. The observed proton thus must be the exchangeable, H-3 proton on the N-3 of exogenous imidazole. In cytochromes b_5 and a, we found no evidence for such a well-resolved, exchangeable proton.

Imidazole Proton ENDOR—Discussion. The known NMR-determined contact interactions[9] of −0.93 and −0.27 MHz for H-2 and H-5, respectively, are certainly less than the ENDOR fre-

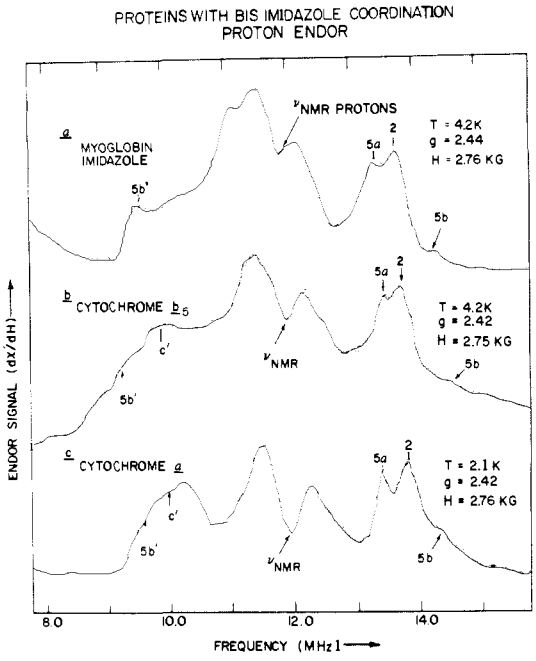

Figure 10. Comparison of proton ENDOR from proteins known (MbIm, cytochrome b_5) or thought (cytochrome *a*) to have bis(imidazole) coordination. Peaks which bear similarity in frequency and/or appearance to those obtained from imidazole protons of H-2 and H-5 of imidazole in $(TPP)Fe(Im)_2^+$ are accordingly labeled in the same manner as the assigned protons from the $(TPP)Fe(Im)_2^+$ complexes of Figure 8. Conditions were similar to those for Figure 8.

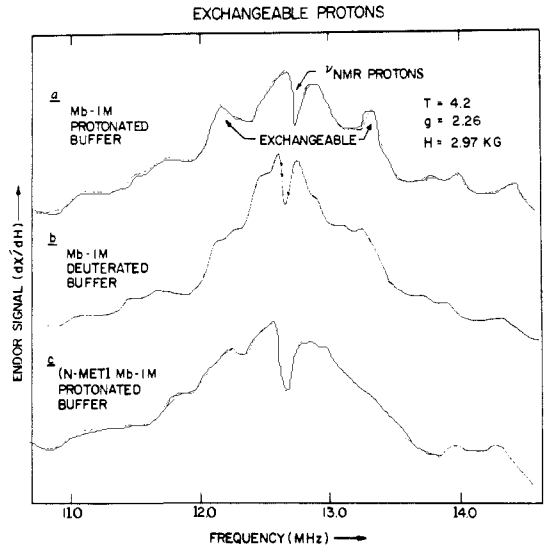

Figure 11. ENDOR from exchangeable H-3 proton of exogenous imidazole in MbIm. Spectra were obtained near $g_y = 2.26$ and with a small field modulation of 0.4 G p.t.p. Each spectrum took about 5 min of signal averaging: (a) proton ENDOR of MbIm prepared in standard *protonated* buffer and with protonated imidazole; (b) proton ENDOR of MbIm prepared with *deuterated* buffer and with protonated imidazole; (c) proton ENDOR of MbIm prepared with *N*-methylimidazole and in protonated buffer.

quencies or first-order hyperfine couplings (fourth column, Table III) of H-2 and H-5. Since H-2 and H-5 are both about 3.2 Å from the heme iron, a substantial dipolar coupling of these protons to the electron spin on the iron is expected. The vector from the heme Fe to either of these protons makes an angle of about 40° to the heme normal. If the magnetic field should lie near the Fe-proton vector, or perpendicular to it, then the magnetic field will lie near a principal hyperfine axis, and better resolved, intense ENDOR peaks will result. Better resolved ENDOR from H-2 and H-5 should and does occur for *g* values that put the magnetic field at 40° or greater to the heme normal; these *g* values are roughly less than 2.7. Since g_z is along the heme normal, ENDOR measurements near $g_z \approx 2.9$ are well away from a principal hyperfine axis of H-2 and H-5, and this explains the poor ENDOR resolution near g_z for H-2 and H-5.

Using eq 5, we can approximately estimate the dipolar interaction for H-2 and H-5, either parallel to ($\theta = 0°$) or perpendicular to ($\theta = 90°$) the Fe-proton vector. In this estimate, we take $r = 3.2$ Å and take $g = 2.5$ as the *g* value in eq 5; 2.5 happens to be a *g* value where good overall resolution of H-2 and H-5 features occurs. This procedure gives estimated dipolar coupling, A_{dip}, of 6.0 MHz parallel to the Fe-proton vector and dipolar coupling, $-^1/_2A_{dip}$, of −3.0 MHz perpendicular to the Fe-proton vector. To obtain the overall estimated couplings parallel, $A_\parallel$, and perpendicular, $A_\perp$, to the Fe-proton bond, we add the appropriate contact interaction to the dipolar interaction. The parallel interaction, $A_\parallel = A_{dip} + A_{con}$, would then be 5.7 and 5.1 MHz, respectively, for H-5 and H-2. The magnitude of $|A_\perp| = |^1/_2A_{dip} + A_{con}|$ would be 3.27 and 3.93 MHz, respectively, for H-5 and H-2. Thus, we expect the hyperfine coupling for H-5 to be greater than that of H-2 when the magnetic field lies near the Fe-proton vector but to be less in magnitude when the magnetic field is perpendicular to the Fe-proton vector.

How do we correlate the estimates of $A_\parallel$ and $A_\perp$ just made with the experimental observations? It is logical that a surface of constant *g* should rarely contain the Fe-to-proton vector for H-2 and H-5 but should more often intersect the plane perpendicular to that Fe-proton direction. Thus, the outlying ENDOR features with the largest hyperfine couplings that would correspond to the magnetic field along the Fe-proton vector are not often observed. The outlying features that were best observed with the largest splittings were at $g = 2.58$, and these gave couplings which we take as the experimental estimates of $A_\parallel$. These experimental estimates of $A_\parallel$ are, respectively, 5.3 MHz for H-5 and 4.2 MHz for H-2. (The H-5 features labeled 5b and 5b′ in Figure 8 also appear to arise from an orientation of the magnetic field near the Fe-proton vector.) The less strongly coupled peaks that occur as well-resolved features over a wider *g*-value range, e.g., 5a, 5a′, 2, 2′ in Figure 8, gave the experimental estimates of $A_\perp$ couplings which were 3.16 and 3.75 MHz for H-5 and H-2, respectively. We thus found that the experimentally determined dipolar coupling, A_{dip}, would be 5.2 and 5.7 MHz for H-2 and H-5, respectively, vs. a predicted value of 6.0 MHz. Our respective experimentally determined contact interactions for H-2 and H-5 would be −1.1 and −0.3 MHz vs. NMR values of −0.93 and −0.27 MHz. The agreement between experiment and this present simple theory could be somewhat improved if there were a 10% decrease in the calculated dipolar interaction due to covalent loss of the electron spin away from the heme iron out to the pyrrole periphery.

A truly quantitative explanation for the appearance of H-2 and H-5 ENDOR spectra as seen at intermediate *g* values like 2.4 and for the relation of imidazole orientation to ENDOR frequencies at these *g* values would require the angle-selected ENDOR theory being developed by Kreilick and co-workers.[27a,b] First-order expressions for ENDOR frequencies of dipolar origin are somewhat invalid at *g* values away from principal *g* axes, especially for strongly coupled protons whose hyperfine couplings are comparable to their Zeeman energies. The overall dipolar tensor (eq 3) should be diagonalized to find nuclear energy levels because the directions for electron spin quantization, applied magnetic field, and nuclear spin quantization are not colinear. First-order theory implicitly assumes the colinearity of these directions. In addition, at a particular *g*-value the resultant pattern of ENDOR frequencies should be summed over all orientations giving rise to that *g*-value.

As shown in Figure 9, we continued to resolve hyperfine couplings from H-2 and H-5 as we went to smaller *g*-values near g_x. The coupling for H-2 was the larger coupling. Given the known negative signs and magnitudes of the NMR-determined contact coupling to H-2 and H-5,[9] it is hard to explain the larger coupling to H-2 and its good ENDOR resolution unless g_x lies largely perpendicular (at least within 20°) to the imidazole plane(s) from

which the H-2 and H-5 ENDOR signals in Figure 9 emanate. If g_x is perpendicular to this imidazole plane, then the dipolar contribution to coupling would be about −1.9 mHz (as opposed to a positive coupling if g_x is parallel to the plane). The calculated magnitudes of the hyperfine coupling to H-2 and H-5 would be 2.8 and 2.2 MHz, to be compared with the experimentally measured 2.6 and 1.8 MHz. In MbIm, the exogenous imidazole lies so that the normal to its plane makes an angle of about 24° to the g_x direction. Thus, for $(TPP)Fe(Im)_2^+$ and MbIm, there is evidence that g_x is close to the normal to an imidazole plane so that if it is π bonding to the imidazole that removes the degeneracy of the d_{xz} and d_{yz} orbitals, then it would be π back-bonding to the d_{xz} orbital that lowers the energy of that orbital with respect to the d_{yz} orbital.

In proteins where the concentration of the paramagnetic centers is highly limited and many proton resonances overlap, NMR sensitivity for H-2 and H-5 is low. Thus, ENDOR seems the method of choice for observing strongly hyperfine-coupled imidazole protons, particularly for high molecular weight proteins like cytochrome *a*. Since protein is thought to modulate heme electronic behavior through the histidine-to-Fe bond, the ENDOR spectra like those of Figure 10 may give important clues to this modulation through its different effect in different proteins. We believe that there is considerable structural information in the overall behavior of imidazole proton ENDOR as a function of *g* values. We look for the overall angle-selected ENDOR technique to give more complete insight into the precise physical causes for differences in imidazole spectra between proteins.

The protons on C-4 and N-3 (called H-4 and H-3) are both about 5.2 Å from the heme iron, and they lie away from the heme normal by about 15°. Contact interactions are, respectively, −0.4 and −0.25 MHz for H-3 and H-4.[9] We have computed first-order hyperfine coupling magnitudes for H-3 and H-4 that are in the range 1.1-1.3 MHz at g_z, 0.9-1.1 MHz at g_y, and 0.7-0.9 MHz at g_x. Unfortunately this means that the ENDOR from these protons generally overlaps with the ENDOR from porphyrin protons. However, there should be no confusion of ENDOR signals between H-4 and H-5 because the H-5 protons are much more strongly hyperfine coupled than H-4; it is for this reason that we have assigned the strongly coupled proton ENDOR in Figure 8d to H-5 even though H-4 is also protonated. The most obvious case where the ENDOR from exchangeable proton N-3 could be assigned was with MbIm for Figure 11 spectra taken near g_y. Taking g_y as approximately perpendicular to the Fe-proton vector of H-3, we computed its dipolar coupling of −0.7 MHz. On adding the H-3 contact interaction[9] to the dipolar contribution, we predicted for H-3 a coupling whose magnitude was 1.1 MHz, to be compared with 1.2 MHz measured by ENDOR. We are not sure why this exchangeable H-3 proton should be so clearly distinguishable by ENDOR only in MbIm; perhaps the exogenous imidazole to which it belongs is rigidly oriented through bonding to the endogenous distal histidine.

Acknowledgment. This work was supported by Grant AM-17884 from the National Institute of Arthritis, Metabolism and Digestive Diseases, Grant GM 35103 from the National Institute of General Medical Sciences, and Grant RR07122 from the Biomedical Research Support Grant Program, Division of Research Resources, NIH. We are grateful to J. L. De Jesus-Collazo and C. Fan for performing calculations related to proton ENDOR interpretation, to H. Taylor for technical assistance in performing the ENDOR measurements, and to Prof. R. Kreilick, University of Rochester, and co-workers for discussions on the angle-selected ENDOR method.

Carcinogenic Alkylation of Nucleic Acid Bases. Structure and Conformation of O^4-Ethyl-2′-deoxythymidine in the Solid State and in Solution[1]

George I. Birnbaum,*[2a] Krishan L. Sadana,[2b] Wayne J. P. Blonski,[2b] and Frank E. Hruska*[2b]

Contribution from the Division of Biological Sciences, National Research Council of Canada, Ottawa, Ontario, Canada K1A 0R6, and the Department of Chemistry, University of Manitoba, Winnipeg, Manitoba, Canada R3T 2N2. *Received August 14, 1985*

Abstract: O^4-Ethyl-2′-deoxythymidine (e^4dT) crystallizes in the monoclinic space group $P2_1$, and the cell dimensions are a = 5.079 (1) Å, b = 15.054 (1) Å, c = 8.467 (1) Å, β = 94.07 (1)°. X-ray intensity data were measured with a diffractometer, and the structure was solved by direct methods. Least-squares refinement, which included all hydrogen atoms, converged at R = 0.030 for 1365 observed reflections. The *O*-ethyl group is coplanar with the pyrimidine ring, the methylene carbon atom being syn to N3. It is shown that O^4-alkylation causes significant changes in the geometry of the ring which can be attributed to an altered electronic structure. The conformation about the glycosidic bond is anti with χ_{CN} = 22.8°. The deoxyribose ring adopts the unusual C3′ endo/C2′ exo twist pucker, and the gauche$^+$ rotamer of the CH_2OH side chain is stabilized by an intramolecular C6—H···O5′ hydrogen bond. Proton NMR data for e^4dT and e^4dU reveal the usual preference for the C2′ endo sugar pucker and a conformer distribution for the C4′-C5′ bond which is expected for 2′-deoxyribosides. Comments are made on the relevance of the structure to base mispairing of *O*-alkyl pyrimidines and their enzymatic repair.

Alkylating agents are known to be mutagens and carcinogens by virtue of their reactions with various nucleophilic sites of DNA.[3] Following early interest in N7-alkylation of guanine,[4,5] considerable attention shifted to O-alkylation of the nucleic acid bases when Loveless[6] prepared O^6-alkyl guanosine and proposed that it might form atypical base pairs. The pyrimidine bases can be alkylated at either the O2 or O4 positions,[3] but there remains uncertainty as to the behavior of the altered bases during transcription and replication. In the case of O^4-alkyl thymine, Abbott and Saffhill[7] suggested the incorporation of dGMP, using randomly methylated poly(dA-dT) as a template. Singer et al.[8] prepared O^4-methyldeoxythymidine (m^4dT) which was then incorporated into a poly(dA-dT) template. Mispairing of m^4dT with guanosine was proven unambiguously by copying the synthesized polymers with DNA polymerase I. Singer et al.[8] also showed that the misincorporation of m^4dT in place of dT does not distort the helical structure of DNA. Consequently, it is important to determine exactly the electronic, hydrogen bonding, and conformational properties of nucleosides with O-alkylated bases. So far, only O^4-methyluridine (m^4U)[9,10] and 6-methoxypurine riboside (O^6-

(1) Issued as NRCC No. 25419.
(2) (a) National Research Council of Canada. (b) University of Manitoba.
(3) Singer, B.; Kušmierek, J. T. *Annu. Rev. Biochem.* **1982**, *51*, 655-693.
(4) Brookes, P.; Lawley, P. D. *Biochem. J.* **1961**, *80*, 496-503.
(5) Fraenkel-Conrat, H. *Biochim. Biophys. Acta* **1961**, *49*, 169-180.
(6) Loveless, A. *Nature (London)* **1969**, *223*, 206-207.
(7) Abbott, P. J.; Saffhill, R. *Nucleic Acids Res.* **1977**, *4*, 761-769.
(8) Singer, B.; Sági, J.; Kušmierek, J. T. *Proc. Natl. Acad. Sci. U.S.A.* **1983**, *80*, 4884-4888.

0002-7863/86/1508-1671$01.50/0